

Nuclear IMPDH filaments in human gliomas

Narges Ahangari, MD,

Department of Pathology, St. Michael's Hospital, Toronto, Ontario, Canada

David G. Munoz, MD,

Department of Pathology, St. Michael's Hospital, Toronto, Ontario, Canada

Josee Coulombe, PhD,

Center for Cancer Therapeutics, Ottawa Hospital Research Institute, Ottawa, Ontario, Canada

Douglas A. Gray, PhD,

Center for Cancer Therapeutics, Ottawa Hospital Research Institute

Elizabeth C. Engle, MD,

Departments of Neurology and Ophthalmology, Boston Children's Hospital and Harvard Medical School, Boston, MA, USA

Long Cheng, PhD,

Department of Neurology, Boston Children's Hospital and Harvard Medical School, Boston, MA, USA

John Woulfe, MD PhD

Center for Cancer Therapeutics and Neurosciences, Ottawa Hospital Research Institute and Department of Pathology and Laboratory Medicine, University of Ottawa

Abstract

The analysis of nuclear morphology plays an important role in glioma diagnosis and grading. We previously described intranuclear rods (rods) labelled with the SDL.3D10 monoclonal antibody against class III beta-tubulin (TUBB3) in human ependymomas. In a cohort of adult diffuse gliomas, we identified nuclear rods in 71.1% of IDH mutant lower grade gliomas and 13.7% of IDH wild type glioblastomas. The presence of nuclear rods was associated with significantly longer post-operative survival in younger (< 65) glioblastoma patients. Consistent with this, nuclear rods were mutually exclusive with Ki67 staining and their prevalence in cell nuclei inversely correlated with the Ki67 proliferation index. In addition, rod-containing nuclei showed a relative depletion of lamin B1, suggesting a possible association with senescence. To gain insight into their functional significance, we addressed their antigenic properties. Using a TUBB3-null mouse model, we demonstrate that the SDL.3D10 antibody does not bind TUBB3 in rods but recognizes an unknown antigen. In the present study, we show that rods show immunoreactivity for the nucleotide synthesizing enzymes inosine monophosphate dehydrogenase (IMPDH) and cytidine triphosphate synthetase (CTPS). By analogy with the IMPDH filaments that have been described

previously, we postulate that rods regulate the activity of nucleotide-synthesizing enzymes in the nucleus by sequestration, with important implications for glioma behavior.

Keywords

Glioma; glioblastoma; nuclear rods; IMPDH filaments; cytoophidia

Introduction:

Despite significant progress in elucidating the molecular mechanisms underlying gliomagenesis, clinical progression with malignant transformation continue to define the natural history of gliomas (1). Therapeutic targeting of class-defining molecular changes is a rational approach to treatment but has produced limited success in terms of improving survival and preventing recurrence. There is recent evidence that non-genetic features, including histopathological ones, segregate with certain epigenetically-defined tumour subgroups with distinct prognostic trajectories (2). Thus, the identification of additional morphological markers which can supplement molecular genetics may contribute to the evolution of a more granular brain tumour classification. Alterations in nuclear morphology have contributed substantially to our understanding of the biology of tumour behavior. Indeed, the assessment of nuclear dysmorphia is commonly employed in the pathological grading of tumours (3). In addition, structural and numeric alterations in a variety of membraneless nuclear organelles, including nucleoli, Cajal bodies, promyelocytic leukemia protein nuclear bodies, and others, provide information regarding tumour behaviour (4).

We have described rod-shaped intranuclear bodies (rods) immunoreactive for class III beta tubulin (TUBB3) in human neurons (5), ependymal cells (5), and pancreatic beta cells (6), as well as in human ependymomas (7). We also identified them in astrocytomas and oligodendrogliomas. The latter finding was surprising because, unlike non-neoplastic ependymal cells, rods are not present in non-neoplastic astrocytes and oligodendrocytes (5). Thus, their presence in these gliomas implies a specific role for these structures in a neoplastic context in these cell types. Understanding the biological significance of these structures is predicated on elucidating their biochemical composition. Although rods show intense staining for the neuron-specific tubulin isoform class III β -tubulin (TUBB3) using the SDL.3D10 monoclonal antibody (SDL), they do not stain for other antibodies generated against TUBB3, nor for antibodies against pan- β -tubulin, suggesting that they are composed of an unrelated antigen. There is precedence for cross-reactivity of the SDL.3D10 antibody with an unknown antigen in an unusual cellular structure similar to rods. "Loukoumasomes" are large annular or linear cytoplasmic structures that were originally described in the cytoplasm of rat sympathetic ganglion neurons (8). Like rods, loukoumasomes stain intensely for SDL.3D10, but not for other antibodies against TUBB3 or pan β -tubulin. Loukoumasomes, in turn, are morphologically identical to cellular structures variably referred to as "cytoophidia" or "rods and rings" (reviewed in (9, 10)). These filamentous structures consist of polymeric assemblies of the nucleotide-synthesizing enzymes inosine monophosphate dehydrogenase (IMPDH) or cytidine triphosphate synthetase (CTPS). On

the basis of these inter-relationships, we reasoned that rods might be antigenically related to these structures and possibly immunoreactive for IMPDH and CTPS.

In the present study, we investigate the presence of nuclear rods in a cohort of human gliomas and compare their prevalence among oligodendrogliomas, astrocytomas, and glioblastomas (GBMs). We correlate their presence with cellular markers of proliferation and, in GBMs, examine their relationship with post-operative survival. In order to gain mechanistic insight, we address the antigenic profile of rods with respect to TUBB3, IMPDH and CTPS. The results of these studies reveal a novel morphological feature of gliomas with important implications for understanding non-genetic determinants of their biological and clinical behavior.

Materials and Methods:

Study Cohort:

All studies were performed in accordance with the ethical guidelines of the Ottawa Hospital Research Institute and St. Michael's Hospital, respectively. Tissue microarrays (TMAs) were prepared using a manual tissue microarrayer (Leica Microsystems, Inc., Wetzlar, Germany.) from representative formalin-fixed, paraffin-embedded blocks of glioma tissue recovered from the tissue archives in the Departments of Pathology of The Ottawa Hospital and St. Michael's Hospital. The co-hort consisted of 37 IDH mutant, 1p/19q co-deleted oligodendrogliomas (16 grade 2, 21 grade 3), 22 IDH mutant, ATRX mutant astrocytomas (12 grade 2, 10 grade 3) and 87 IDH wild type GBMs.

TUBB3^{-/-} mouse brain processing:

TUBB3^{-/-} mice were previously generated and kindly provided by Drs. Elizabeth Engle and Long Cheng, Boston Children's Hospital and Harvard Medical School, Boston, MA, USA (11). Adult *TUBB3*^{-/-} mice were intracardially perfused with 10% neutral formalin, the skull removed, and the brains carefully dissected. Brains were then fixed in 10% neutral formalin for 24-48 hr and processed for embedding in paraffin. Serial sections at 5 mm thickness were collected and mounted on superfrost-coated slides (Fisher Scientific, Pittsburgh, PA, USA).

Immunostaining:

The primary antibodies employed are listed in Table 1. For double-labelling immunofluorescence studies, following incubation in the primary antibodies, TMAs were incubated in a cocktail of goat-anti mouse and goat anti-rabbit secondary antibodies conjugated to Alexafluor 488 and 594 fluorescent tags (ThermoFisher, Waltham, MA, USA). TMAs were coverslipped using aqueous mounting media containing 1.5 µg/ml 4',6-diamidino-2-phenylindole (DAPI) as a nuclear counterstain (Vector Laboratories, Burlingame, CA, USA).

Microscopy:

Microscopic imaging was performed in the Cell Biology and Image Acquisition core facility at The University of Ottawa. High resolution microscopic imaging was performed using a

Zeiss 880 Confocal Microscope with Airyscan Fast (Zeiss, Oberkochen, Germany). TMAs stained for SDL, SDL/Ki67, SDL/Lamin B1, and SDL/Lamin A/C were scanned using a Zeiss M1 Slide Scanner with fluorescence capability (Zeiss, Oberkochen, Germany).

Electron microscopy:

Tissue was fixed in sodium cacodylate buffered 2.5% glutaraldehyde (Electron Microscopy Sciences, Hatfield, PA, USA), dehydrated through graded ethanol and acetone and embedded in Spurr's resin (Ted Pella, Inc., Mountain Lakes CA, USA). Eighty nm thin sections were mounted onto copper grids Ted Pella, Inc. Mountain Lakes CA, USA), and examined with a Hitachi H 7100 transmission electron microscope (Hitachi, Tokyo, Japan).

Data Analysis:

Image analysis was performed on digital images using Zeiss Zen (Zeiss, Oberkochen, Germany) and Fiji (12) software. For quantitative analysis of rod frequency and Ki67 index in double-stained images for SDL and Ki67, an area of 200 μ m X 200 μ m was selected randomly in each image. The total number of nuclei in the selected area was calculated by Fiji software and the number of nuclei containing rods was counted manually. Rod frequency was defined as the proportion of nuclei with rods. The same procedure was used for Ki67 index calculation.

Nuclear and cytoplasmic intensity of Lamin B1 and Lamin A/C staining were analyzed using Fiji software. For this analysis, 15 nuclei with rods and 15 nuclei without rods were selected randomly in each image.

All the statistical analyses were done using SPSS Statistics 24.0 statistical software (IBM, Chicago, IL, USA). The χ^2 test was used for categorical variables. The Kolmogorov-Smirnov test of normality was statistically significant thus non-parametric tests were used for analysis. The Mann-Whitney U test, Spearman's rank correlation, and linear regression analysis were used for continuous data. The significance level was set at $\alpha=0.05$. Kaplan-Meier Survival analysis was performed to investigate the effect of nuclear rods on post-operative survival among 83 of 87 GBM patients with available survival data. Further survival analysis was also done on stratified data based on age and sex to analyze the effect of these factors. All Kaplan-Meier survival curves were reported with a P value obtained from log-rank test. All statistical analyses were conducted using a $\alpha = 0.05$ significance.

Results:

Morphology

Rod-shaped structures were identified within the nuclei of tumour cells in a large proportion of gliomas. A small number could be seen in hematoxylin and eosin stained sections where they appeared as a linear "gap" in hematoxylin staining containing a slightly eosinophilic "blush" (Figure 1A). As reported previously, these rods stained intensely using the SDL.3D10 (SDL) monoclonal antibody generated against TUBB3 (5, 7, 13–15) (Figure 1B, C). Rods varied in morphology with the majority consisting of long, thread-like structures, in many cases spanning the entire nuclear diameter (Figure 1B, C). Most rod-

bearing nuclei contained a solitary rod although rare nuclei showed two or even three rods. Longer rods were oriented parallel to the long axis of nuclei (Figure 1C). In addition to the more common straight linear forms, curved linear structures, dot-shaped structures (Figure 1B arrowhead and inset) and sheets (Figure 1B, arrow and inset) were observed. Many appeared to be “hollow” with respect to SDL staining; showing a “bilaminar” appearance in longitudinal, and annular in transverse sectional planes.

By electron microscopy, when viewed in the longitudinal plane (Figure 2A–C) rods consisted of compact, parallel arrays of slightly wavy electron dense filaments measuring from 6 to 10 nm in diameter. When viewed in the transverse plane, they appeared as circular arrays of short, slightly wavy filaments (Figure 2D–F).

Rods are prevalent in IDH mutant oligodendrogliomas and astrocytomas, but not IDH wild type GBMs

Overall, rods were present at various frequencies (0.4–37% of tumour cells) in 71.1% of IDH mutant lower grade gliomas and (13.7%) of IDH wild type gliomas (all GBMs). We employed a semi-quantitative scale to assess the frequency of nuclear rods using 5% and 10% to define four categories with 0, low (0–5%), moderate (5.1–10%), and high (>10%) prevalence. The results for the entire co-hort are summarized in Figure 3A and B. Rods were significantly more prevalent in oligodendrogliomas (78.3%; 81% of grade 2, 76.2% of grade 3) than astrocytomas (59%; 66.7% of grade 2, 50.0% of grade 3) (Figure 3). Among grades 2 and 3 oligodendrogliomas and astrocytomas, there was no significant correlation between the presence or frequency of rods and tumour grade, sex, or tumour site. There was a significant negative correlation between the frequency of rods and age in oligodendrogliomas but no relationship with age in astrocytomas or GBMs. With respect to molecular genetic profile, one tumour with a R172K IDH2 mutation had the highest frequency of rods (Figure 3C). However, overall, tumours with IDH2 (R172K, R172G) or non-canonical IDH1 (R132C, R132G) mutations did not show significant differences in terms of rod frequency (Figure 3C).

To determine whether the presence of rods conferred any prognostic information, we analyzed post-operative survival and recurrence in 83 IDH wild type GBM patients with available data. Post-operative follow-up period ranged from 1 to 910 days. The average post-operative follow-up period was 328 days for rod-positive and 210 days for rod-negative patients. The duration of post-operative follow-up did not differ significantly among the two groups ($p=0.15$). Across all age groups, there was no significant difference in post-operative survival among patients with rod-positive and rod-negative tumours (Figure 3D). However, when patients were stratified by age, the presence of rods conferred significantly improved post-operative survival in those 65 years of age and below (Figure 3E). Stratification by sex revealed no significant effect for rods on post-operative survival.

Rods are a marker of proliferative quiescence in glioma cells

In light of the above findings, we next investigated the relationship between the presence of rods and glioma cell proliferation. Double immunostaining revealed mutual exclusion of rods and the proliferation marker Ki67 (Figure 4A–C). In addition, there was a significant

inverse correlation between the frequency of rods and the Ki67 proliferation index in both oligodendrogliomas (Figure 4D) and astrocytomas (Figure 4E). This suggested that rod formation correlates with cellular proliferative quiescence in glioma cells.

Senescence, the irreversible arrest of cell proliferation (16), represents an important stage in the malignant evolution of glioma cells. To begin to investigate a possible relationship between rod formation and senescence, we performed double labelling for rods using SDL and lamin B1. Lamin B1 is an intermediate filament protein which, along with lamin A/C, forms a meshwork lining the inner nuclear membrane. Reduced nuclear membrane staining for lamin B1 has become an established marker of senescence (17). The intensity of nuclear membrane lamin B1 staining was significantly reduced in rod-containing nuclei relative to their negative counterparts (Figure 5A, B). This phenomenon was selective for lamin B1 as there was no similar reduction for lamin A/C (Figure 5C, D).

Antigenicity: Rods are related to IMPDH filaments

In order to gain insight into the functional significance of rods in glioma cells, we investigated their antigenic properties, focusing first on the specificity of SDL staining for TUBB3. The SDL monoclonal antibody was generated against a synthetic peptide (CESESQGPK) corresponding to the c-terminal tail of TUBB3 (18). However, rods did not stain for other anti-TUBB3 monoclonal antibodies, including the TUJ-1 and TU-20 clones which were generated against an almost identical C-terminal isotype-defining epitope of the protein. They also failed to stain with a polyclonal anti-TUBB3 antibody (Figure 6A–C) as well as an antibody to pan β -tubulin (Figure 6D–F). These results suggested that SDL recognizes something other than TUBB3 in rods. To investigate this, we performed immunostaining studies on the brains of *Tubb3*-null mice. These mice were generated by deleting exon 4, which represents over 80% of the TUBB3 gene and contains the isotype-defining c-terminus, including the SDL epitope (11). Not only were rods detected in neurons of *Tubb3*-null brains using SDL, but the rods were more intensely stained than those in control brains (Figure 6G, H). These results indicate that the SDL antibody recognizes something other than TUBB3 in rods.

There are two isoforms of IMPDH (1 and 2) which share 84% sequence homology, both of which have been described in IMPDH filaments. SDL-immunoreactive intranuclear rods stained for IMPDH using three different anti-IMPDH antibodies including a rabbit polyclonal antibody targeting amino acids 170-235 of IMPDH1 (Figure 7A–C; specificity knockdown validated in (19)) and a rabbit polyclonal antibody targeting amino acids 1-350 of IMPDH2 (specificity knockdown validated in (19, 20)). Lighter staining was observed with a mouse monoclonal antibody targeting amino acids 380-410 and recognizing both IMPDH 1 and 2. Due to the significant sequence homology among the two isoforms, cross-reactivity of the antibodies with the alternate isoforms could not be excluded. Consequently, it was not possible to determine whether IMPDH filaments were comprised exclusively of IMPDH1, 2, or were a mixture of both. Consistent with reports of a nuclear localization of IMPDH, a proportion of glioma cell nuclei also showed diffuse nuclear staining (21). This was especially strong using the rabbit polyclonal anti-IMPDH2 antibody. IMPDH filaments have been described in close association with independent filaments comprised of

the pyrimidine synthesizing enzyme CTPS (22). Like IMPDH, CTPS exists in two isoforms which share 74% sequence homology. A proportion of SDL-immunoreactive rods showed immunostaining for CTPS using a rabbit monoclonal antibody generated against a 13 amino acid synthetic peptide between amino acids 50 and 100 of CTPS2 (Figure 7D–F). CTPS staining appeared to be confined to larger rods. These results suggest that rods are related to nuclear forms of IMPDH- and mixed IMPDH and CTPS filaments.

Discussion:

In the present study, we extend our previous observations in ependymomas to demonstrate the presence of intranuclear SDL-immunoreactive rods in adult diffuse gliomas. In our original study of these structures in the human brain, rods were not present in astrocytes or oligodendrocytes. Thus, their presence in the neoplastic counterparts of these cells indicates that they may have an important role in gliomas.

Using a well-characterized TUBB3-null mouse model, we confirmed that the SDL-immunoreactive moiety in rods is not TUBB3. Instead, rods are immunoreactive for IMPDH, the rate-limiting enzyme in the *de novo* synthesis of GTP and ATP nucleotides. IMPDH catalyzes the NAD⁺-dependent oxidation of IMP to xanthine monophosphate (23). This pivotal step in GMP synthesis controls the size of the guanine nucleotide pool. Thus, IMPDH is a key enzyme for genome replication and cell proliferation. IMPDH activity and GTP abundance are transformation and progression linked in cancer cells (24, 25). Indeed, GTP levels and IMPDH activity are markedly increased in GBM (24, 25). In addition to their role as building blocks to support DNA replication and cell division, purine nucleotides are involved in myriad metabolic and cell signaling functions.

Metabolic regulation via filamentation has been described for an increasing number of enzymes (26). IMPDH filament formation has been implicated as a mechanism to regulate its activity, the direction of which is influenced by substrate availability, allosteric feedback inhibition by nucleotide products, and the identity of the enzyme isoform (27). At least one study has linked filament formation to increased enzymatic activity (28). IMPDH filaments have been described predominantly in the cytoplasm where their formation can be potently induced by a variety of stimuli, including pharmacological inhibitors (reviewed in (9, 10)). Nuclear forms have also been described, although their functional significance is less well studied. Based on their morphological similarity as well as their immunoreactivity for IMPDH and CTPS, we postulate that nuclear rods in glioma cells are related in some way to nuclear IMPDH filaments. It will be important to identify the SDL-immunoreactive antigen in this context as an increasing number of proteins have been identified in IMPDH filaments, including the small GTPase ARL2 complexed with the tubulin binding cofactor D, suggesting possible roles for these structures beyond nucleotide regulation, including microtubule dynamics (29). It is also possible that IMPDH- and SDL-based filaments are independent entities but are physically juxtaposed. This has been described for IMPDH- and CTPS-based filaments and may reflect a mechanism for the co-ordinated regulation of purine and pyrimidine synthesis (30). The presence of IMPDH in rods has important implications for understanding the associations we have demonstrated in

this study, including that between rods and IDH-mutant gliomas, reduced proliferation, and increased survival in a subset of GBM patients.

The prevalence of rods in oligodendrogliomas versus astrocytomas and GBMs may be related to differential metabolic profiles. Specifically, as a critical substrate in the *de novo* purine nucleotide synthetic pathway, it is not surprising that changes in the concentration of glutamine markedly influence IMPDH filamentation, with glutamine depletion and supplementation inducing and reversing filament formation, respectively (31). This is compelling in the context of our previous studies showing rods in human pancreatic beta cells which were significantly reduced in diabetic subjects (32) as glutamine is present in high concentrations in β cells and is a powerful insulin secretagogue (33). Interestingly, this effect is dependent on IDH (34). Glutamine is also essential for cancer cells to fuel nucleotide and nucleic acid synthesis for proliferation. Indeed, the reliance of malignant cells on glutamine (glutamine “addiction”) has been implicated as a therapeutic target (35). In this context, rod formation may represent a glutamine-related metabolic signature in gliomas. Consistent with this, the ordinal prevalence of rods (oligodendrogliomas > astrocytomas > GBMs) correlates with relative glutamine levels among these tumour types. Relative to IDH wild type GBMs, IDH mutant gliomas show suppressed levels of glutamate and in turn are more reliant on glutaminase, which catalyzes the production of glutamate at the expense of intracellular glutamine (36). In addition, there are significant differences in the metabolic signatures among oligodendrogliomas and astrocytomas, including glutamine concentrations (37). Significant metabolic differences have also been described among IDH mutant gliomas with R132H versus non-canonical or IDH2 mutations (38). With the evolution of an increasingly granular sub-classification of adult diffuse gliomas, it will be interesting to determine whether the presence of rods characterizes novel metabolic subclasses across molecular groups. Along the same lines, determining whether rod-positive and -negative gliomas form distinct subclusters within individual glioma groups using epigenetic (methylation) profiling may be informative.

Our study provides evidence for an inverse relationship between nuclear rod formation and glioma cell proliferation. That rod prevalence decreases along the established hierarchical scale of increasingly aggressive tumour behavior (oligodendroglioma > astrocytoma > GBM) is consistent with this. Although the significance of nuclear IMPDH filaments is unknown, IMPDH has been shown to accumulate in the nucleus in a cell cycle dependent manner where it “moonlights” as a transcription factor to influence proliferation in either direction (21). Interestingly, nuclear IMPDH attenuates expression of histone genes and E2F, a key driver of cell proliferation (21). E2F plays a central role in the induction of senescence (39–41). By influencing IMPDH activity in the nucleus through physical sequestration, rod formation may reflect an intranuclear regulatory mechanism impacting cell proliferation. The relationship between rods and lamin B1 depletion, an established morphological marker of senescence (42), is interesting in this regard, and suggests a possible role for nuclear rod formation in senescence. These findings also have implications for glioma prognosis. Consistent with their correlation with reduced proliferation, the presence of rods portended a significantly more favourable prognosis in terms of post-operative survival for patients with IDH wild type GBM who were under 65 years of age at the time of surgery. The absence of

an association in elderly patients may reflect the presence of age-associated co-morbidities contributing to mortality.

This study has potential therapeutic implications. IMPDH has a long history as an attractive anti-neoplastic target (43). Notably, IMPDH-targeting drugs (9) have been demonstrated to influence IMPDH-filament formation. The development of next generation, more efficacious IMPDH-targeting drugs is ongoing (43) and is predicated on a more nuanced understanding of IMPDH regulation in glioma cells. A salient example is the recent study by Shireman and co-workers who demonstrated an interaction between IMPDH and the ciliary GTPase ARL13B, a negative regulator of purine salvage (44). Inhibition of this interaction using the FDA approved drug mycophenolate mofetil (MMF) enhanced temozolamide-induced DNA damage by forcing cells to rely on purine salvage. The authors suggested that MMF and temodol may be effective as a combination therapy. In addition to providing insight regarding mechanisms of action, assessment of rod prevalence in resected tissue specimens may provide information regarding the response to treatment. Our findings may also have implications for the development of anti-glioma immunotherapies. In hepatitis patients treated with the antiviral drug ribavirin, IMPDH filaments form in peripheral blood mononuclear cells. Remarkably, drug-induced filament formation in these patients initiates a robust autoimmune response with the development of autoantibodies targeting IMPDH (45). It will be interesting to determine whether patients with rod-bearing gliomas harbor such autoantibodies and whether this autoantigenic property can be leveraged for the development of novel anti-glioma immunotherapies.

We have described a novel morphological feature in human adult diffuse gliomas. Future studies will provide mechanistic insight regarding the functional significance of rods and their role in IMPDH regulation and glioma behavior. In addition to informing future fundamental studies, the results of our studies have clinical relevance. Our study indicates that rods represent a morphological marker of reduced glioma cell proliferation and that their presence in glioma specimens has prognostic value in patients with GBM. Thus, evaluation of rods in resected glioma tissue may supplement the diagnostic arsenal available to neuropathologists to convey prognostic information to treating clinicians. Further understanding of the protein composition and functional significance of rods in gliomas, as well as the immune response to these structures, could foster the development of novel therapeutic approaches.

Support:

JW is supported by The Joan Sealy Trust of the Ottawa Hospital Research Institute. ECE is a Howard Hughes Medical Institute Investigator.

References

1. Marenco-Hillebrand L, Wijesekera O, Suarez-Meade P, et al. Trends in glioblastoma: outcomes over time and type of intervention: a systematic evidence based analysis. *JNeurooncol* 2020;147:297–307 [PubMed: 32157552]
2. Fukuoka K, Mamatjan Y, Tatevossian R, et al. Clinical impact of combined epigenetic and molecular analysis of pediatric low-grade gliomas. *Neuro Oncol* 2020;22:1474–83 [PubMed: 32242226]

3. Veltri RW, Partin AW, Miller MC. Quantitative nuclear grade (QNG): a new image analysis-based biomarker of clinically relevant nuclear structure alterations. *J Cell Biochem Suppl* 2000;Suppl 35:151–7
4. Mao YS, Zhang B, Spector DL. Biogenesis and function of nuclear bodies. *Trends Genet* 2011;27:295–306 [PubMed: 21680045]
5. Woulfe J, Munoz D. Tubulin immunoreactive neuronal intranuclear inclusions in the human brain. *Neuropathol Appl Neurobiol* 2000;26:161–71 [PubMed: 10840279]
6. Prichett W, Milman P, Gagnon J, et al. Intranuclear rodlets in human pancreatic islet cells. *Pancreas* 2007;35:207–11 [PubMed: 17895839]
7. Woulfe J Class III beta-tubulin immunoreactive intranuclear inclusions in human ependymomas and gangliogliomas. *Acta Neuropathol* 2000;100:427–34 [PubMed: 10985703]
8. Ramer MS, Cruz Cabrera MA, Alan N, et al. A new organellar complex in rat sympathetic neurons. *PLoS one* 2010;5:e10872 [PubMed: 20531934]
9. Calise SJ, Chan EKL. Anti-rods/rings autoantibody and IMPDH filaments: an update after fifteen years of discovery. *Autoimmun Rev* 2020;19:102643 [PubMed: 32805424]
10. Liu JL. The Cytoophidium and Its Kind: Filamentation and Compartmentation of Metabolic Enzymes. *Annu Rev Cell Dev Biol* 2016;32:349–72 [PubMed: 27362644]
11. Latremoliere A, Cheng L, DeLisle M, et al. Neuronal-Specific TUBB3 Is Not Required for Normal Neuronal Function but Is Essential for Timely Axon Regeneration. *Cell Rep* 2018;24:1865–79 e9 [PubMed: 30110642]
12. Schindelin J, Arganda-Carreras I, Frise E, et al. Fiji: an open-source platform for biological-image analysis. *Nat Methods* 2012;9:676–82 [PubMed: 22743772]
13. Woulfe J, Gray D, Prichett-Pejic W, et al. Intranuclear rodlets in the substantia nigra: interactions with marinesco bodies, ubiquitin, and promyelocytic leukemia protein. *J Neuropathol Exp Neurol* 2004;63:1200–7 [PubMed: 15581187]
14. Woulfe JM, Hammond R, Richardson B, et al. Reduction of neuronal intranuclear rodlets immunoreactive for tubulin and glucocorticoid receptor in Alzheimer's disease. *Brain Pathol* 2002;12:300–7
15. Woulfe JM, Prichett-Pejic W, Rippstein P, et al. Promyelocytic leukaemia-immunoreactive neuronal intranuclear rodlets in the human brain. *Neuropathol Appl Neurobiol* 2007;33:56–66 [PubMed: 17239008]
16. Hayflick L The Limited in Vitro Lifetime of Human Diploid Cell Strains. *Exp Cell Res* 1965;37:614–36 [PubMed: 14315085]
17. Shimi T, Butin-Israeli V, Adam SA, et al. The role of nuclear lamin B1 in cell proliferation and senescence. *Genes Devel* 2011;25:2579–93 [PubMed: 22155925]
18. Banerjee A, Roach MC, Trcka P, et al. Increased microtubule assembly in bovine brain tubulin lacking the type III isotype of beta-tubulin. *J Biol Chem* 1990;265:1794–9 [PubMed: 2404018]
19. Ruan H, Song Z, Cao Q, et al. IMPDH1/YB-1 Positive Feedback Loop Assembles Cytoophidia and Represents a Therapeutic Target in Metastatic Tumors. *Mol Ther* 2020;28:1299–313 [PubMed: 32209435]
20. Keppeke GD, Chang CC, Peng M, et al. IMP/GTP balance modulates cytoophidium assembly and IMPDH activity. *Cell Div* 2018;13:5 [PubMed: 29946345]
21. Kozhevnikova EN, van der Knaap JA, Pindyurin AV, et al. Metabolic enzyme IMPDH is also a transcription factor regulated by cellular state. *Mol Cell* 2012;47:133–9 [PubMed: 22658723]
22. McCluskey GD, Bearne SL. Anfractuous assemblies of IMP dehydrogenase and CTP synthase: new twists on regulation? *FEBS J* 2018;285:3724–8 [PubMed: 30285320]
23. Hedstrom L IMP dehydrogenase: structure, mechanism, and inhibition. *Chem Rev* 2009;109:2903–28 [PubMed: 19480389]
24. Kofuji S, Sasaki AT. GTP metabolic reprogramming by IMPDH2: unlocking cancer cells' fuelling mechanism. *J Biochem* 2020;168:319–28 [PubMed: 32702086]
25. Kofuji S, Hirayama A, Eberhardt AO, et al. IMP dehydrogenase-2 drives aberrant nucleolar activity and promotes tumorigenesis in glioblastoma. *Nat Cell Biol* 2019;21:1003–14 [PubMed: 31371825]

26. Lynch EM, Kollman JM, Webb BA. Filament formation by metabolic enzymes-A new twist on regulation. *Curr Opin Cell Biol* 2020;66:28–33 [PubMed: 32417394]
27. Simonet JC, Burrell AL, Kollman JM, et al. Freedom of assembly: metabolic enzymes come together. *Mol Biol Cell* 2020;31:1201–5 [PubMed: 32463766]
28. Chang CC, Lin WC, Pai LM, et al. Cytoophidium assembly reflects upregulation of IMPDH activity. *J Cell Sci* 2015;128:3550–5 [PubMed: 26303200]
29. Schiavon CR, Griffin ME, Pirozzi M, et al. Compositional complexity of rods and rings. *Mol Biol Cell* 2018;29:2303–16 [PubMed: 30024290]
30. Chang CC, Keppeke GD, Sung LY, et al. Interfilament interaction between IMPDH and CTPS cytoophidia. *FEBS J* 2018;285:3753–68 [PubMed: 30085408]
31. Calise SJ, Carcamo WC, Krueger C, et al. Glutamine deprivation initiates reversible assembly of mammalian rods and rings. *Cell Mol Life Sci* 2014;71:2963–73 [PubMed: 24477477]
32. Zhou YY, El Hallani S, Balaa F, et al. Depletion of Beta Cell Intranuclear Rodlets in Human Type II Diabetes. *Endocrine Pathol* 2017;28:282–6 [PubMed: 28770422]
33. Li C, Buettger C, Kwagh J, et al. A signaling role of glutamine in insulin secretion. *J Biol Chem* 2004;279:13393–401 [PubMed: 14736887]
34. Zhang GF, Jensen MV, Gray SM, et al. Reductive TCA cycle metabolism fuels glutamine- and glucose-stimulated insulin secretion. *Cell Metab* 2021;33:804–17 e5 [PubMed: 33321098]
35. Wise DR, Thompson CB. Glutamine addiction: a new therapeutic target in cancer. *Trends Biochem Sci* 2010;35:427–33 [PubMed: 20570523]
36. McBrayer SK, Mayers JR, DiNatale GJ, et al. Transaminase Inhibition by 2-Hydroxyglutarate Impairs Glutamate Biosynthesis and Redox Homeostasis in Glioma. *Cell* 2018;175:101–16 e25 [PubMed: 30220459]
37. Viswanath P, Batsios G, Mukherjee J, et al. Non-invasive assessment of telomere maintenance mechanisms in brain tumors. *Nat Commun* 2021;12:92 [PubMed: 33397920]
38. Tesileanu CMS, Vallentgoed WR, Sanson M, et al. Non-IDH1-R132H IDH1/2 mutations are associated with increased DNA methylation and improved survival in astrocytomas, compared to IDH1-R132H mutations. *Acta Neuropathol* 2021;141:945–57 [PubMed: 33740099]
39. Popov B, Petrov N. pRb-E2F signaling in life of mesenchymal stem cells: Cell cycle, cell fate, and cell differentiation. *Genes Dis* 2014;1:174–87 [PubMed: 30258863]
40. Dimri GP, Hara E, Campisi J. Regulation of two E2F-related genes in presenescent and senescent human fibroblasts. *J Biol Chem* 1994;269:16180–6 [PubMed: 8206919]
41. Hayflick L, Moorhead PS. The serial cultivation of human diploid cell strains. *Exp Cell Res* 1961;25:585–621 [PubMed: 13905658]
42. Sharpless NE, Sherr CJ. Forging a signature of in vivo senescence. *Nat Rev Cancer* 2015;15:397–408 [PubMed: 26105537]
43. Naffouje R, Grover P, Yu H, et al. Anti-Tumor Potential of IMP Dehydrogenase Inhibitors: A Century-Long Story. *Cancers* 2019;11
44. Shireman JM, Atashi F, Lee G, et al. De novo purine biosynthesis is a major driver of chemoresistance in glioblastoma. *Brain* 2021;144:1230–46 [PubMed: 33855339]
45. Calise SJ, Keppeke GD, Andrade LE, et al. Anti-rods/rings: a human model of drug-induced autoantibody generation. *Front Immunol* 2015;6:41 [PubMed: 25699057]

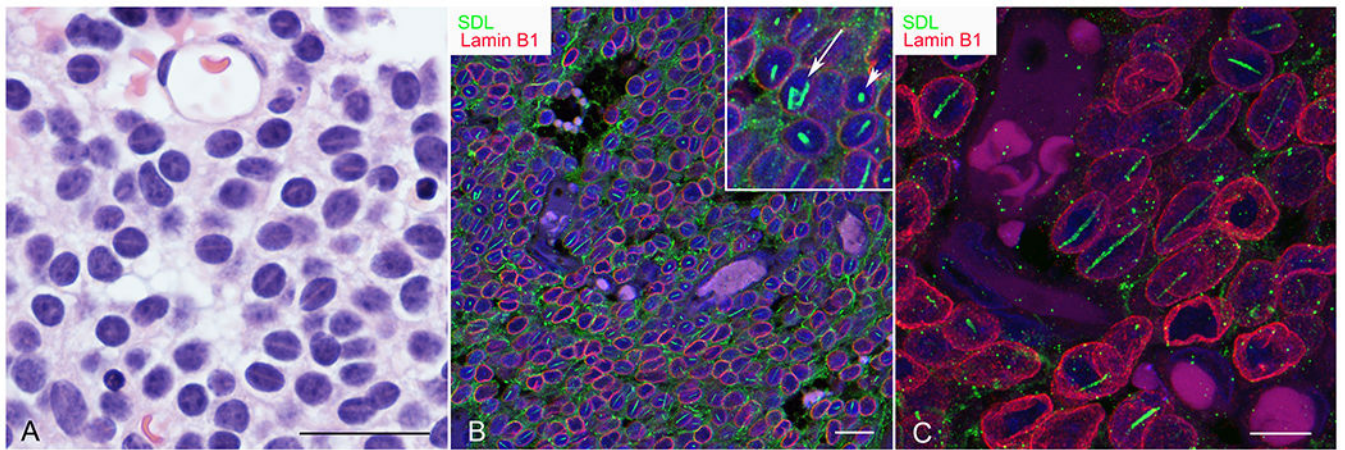


Figure 1:

Rod morphology. A) Rods in this oligodendroglioma are visible as hematoxylin-poor, slightly eosinophilic linear zones in hematoxylin and eosin-stained sections of some tumours. B) Confocal image showing double immunofluorescence staining for SDL (green) and lamin B1 (red) in an oligodendroglioma. The majority of rods are linear. Occasional paracrystalline sheets (arrow shows a curved sheet) and dot-shaped (arrowhead) morphologies are seen (see inset). C) Three-dimensional reconstruction of a confocal z-stack showing rods in an oligodendroglioma at higher magnification. Rods are oriented parallel to the long axis of nuclei. Bars=25 μ m in A, 20 μ m in B and 10 μ m in C.

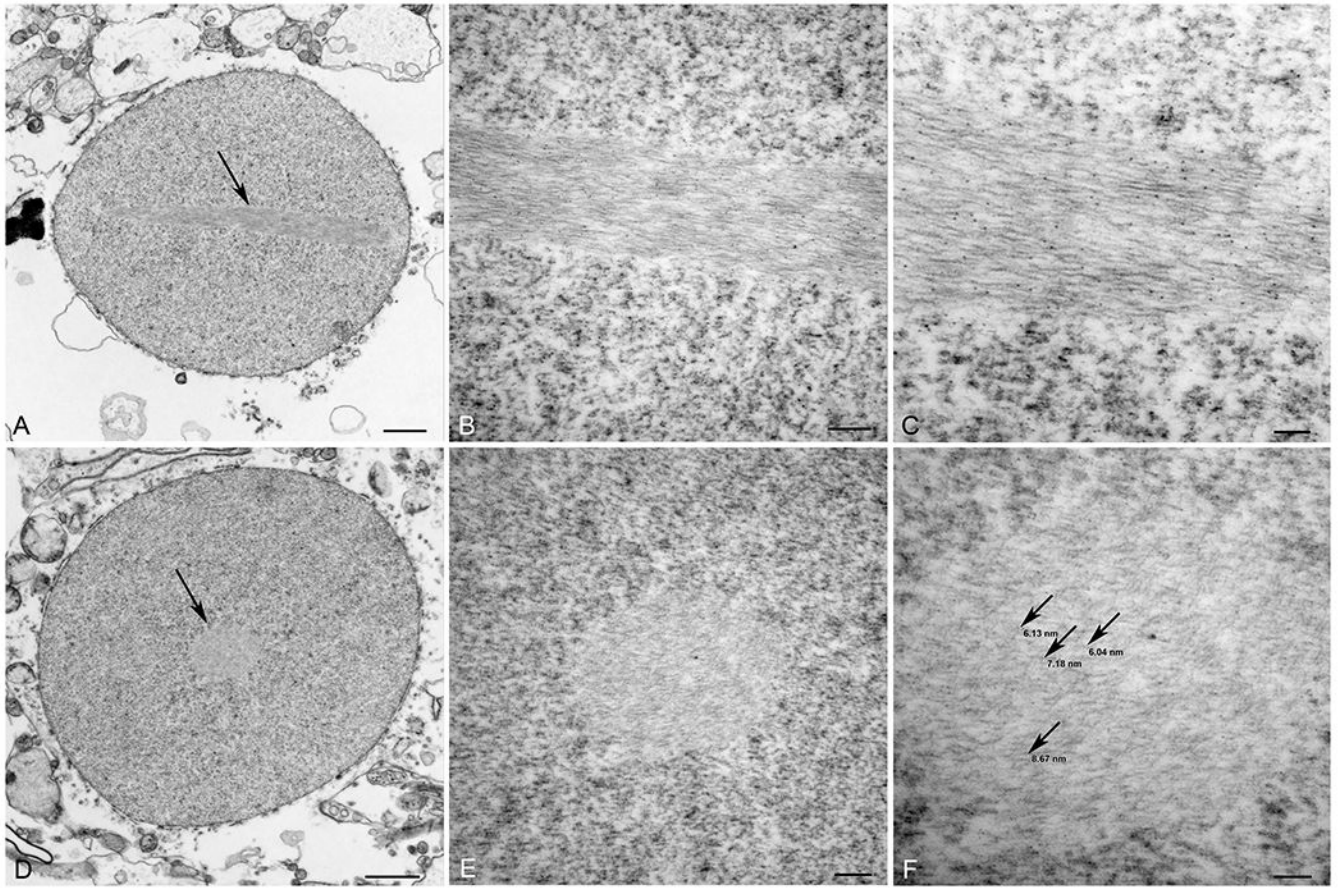


Figure 2: Rod ultrastructure. Electron micrographs showing rods in longitudinal (A-C; arrow in A) and transverse (D-F; arrow in D) planes within nuclei of an oligodendrogloma. The rods consist of parallel arrays of slightly wavy electron dense filaments. Bars=1 μm in A and D, 200 nm in B and E, 100 nm in C and F.

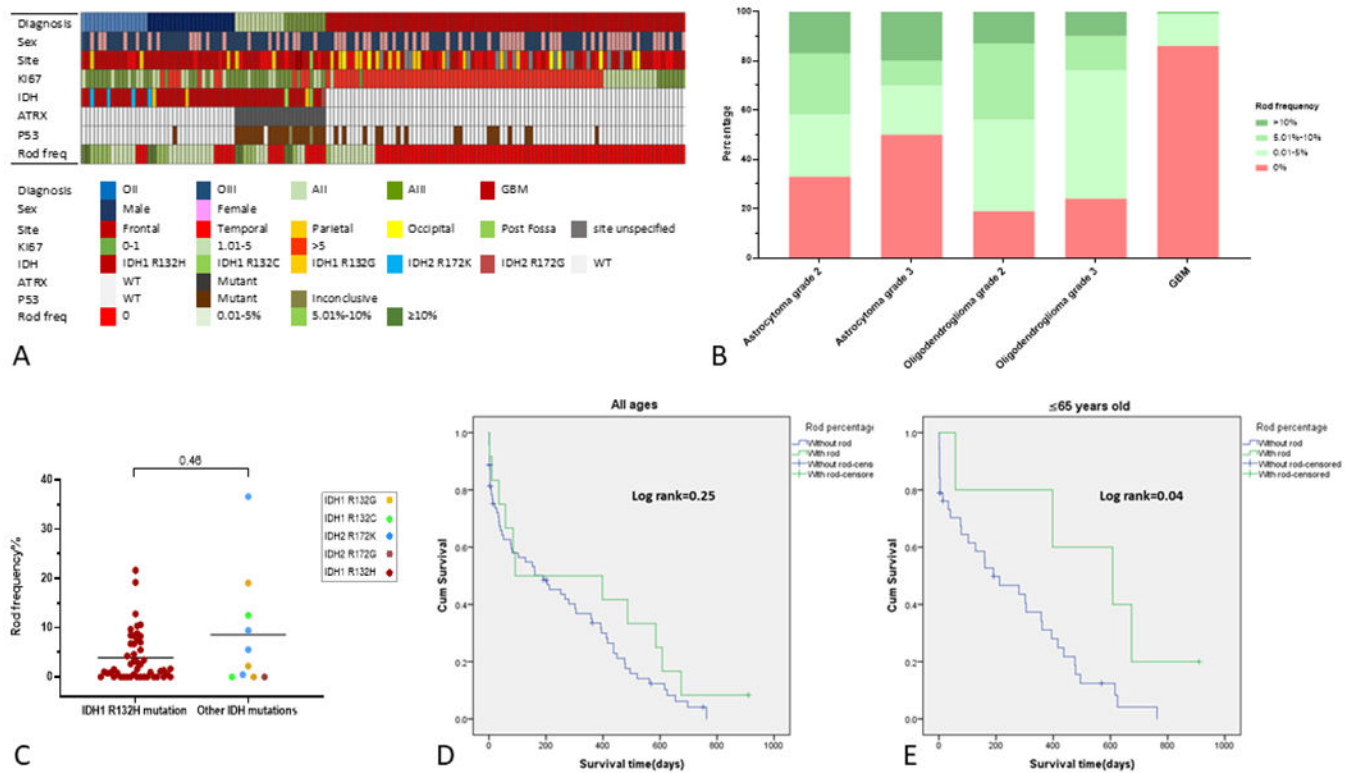


Figure 3:
 A) Oncoprint summarizing demographic features, tumour localization, Ki67 proliferation index, IDH/ATRX/p53 mutation status, and rod frequency (freq) for our entire adult diffuse glioma co-hort. B) Bar graph showing the relative proportion of oligodendrogliomas, astrocytomas, and glioblastomas containing rods. Rod frequency is illustrated semi-quantitatively using 5% and 10% cut-offs into three categories represented by increasingly darker shades of green (pink=no rods). C) Dot plot comparing rod frequencies among gliomas with IDH1R132H mutations and those with IDH2 and non-canonical IDH1 mutations. D, E) Kaplan-Meier analyses comparing post-operative survival among subjects with rod-positive (green) versus rod-negative (blue) IDH wild-type glioblastomas. There was no significant difference in survival among subjects of all ages whereas those 65 years of age and younger with rods exhibited significantly improved survival (E).

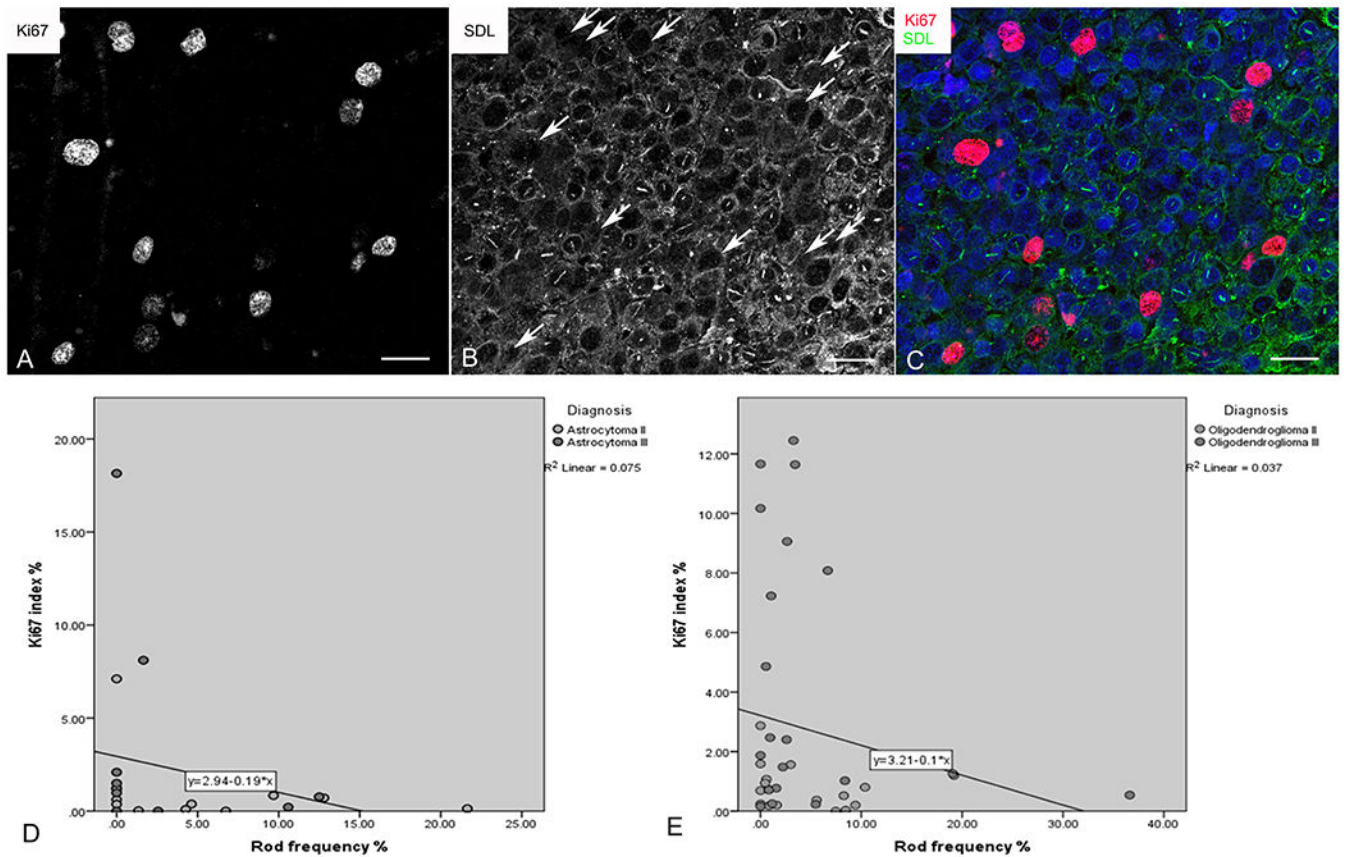


Figure 4:

Inverse relationship between rods and proliferation. A - C) Confocal multichannel image showing Ki67-immunoreactive nuclei (A) lacking rods (B; arrows indicate Ki67-positive nuclei shown in A). The merged pseudocoloured image is shown in C. Bars=20 μm . D, E) Regression analyses showing inverse correlation between Ki67 proliferation index and rod prevalence in astrocytomas (D) and oligodendrogliomas (E).

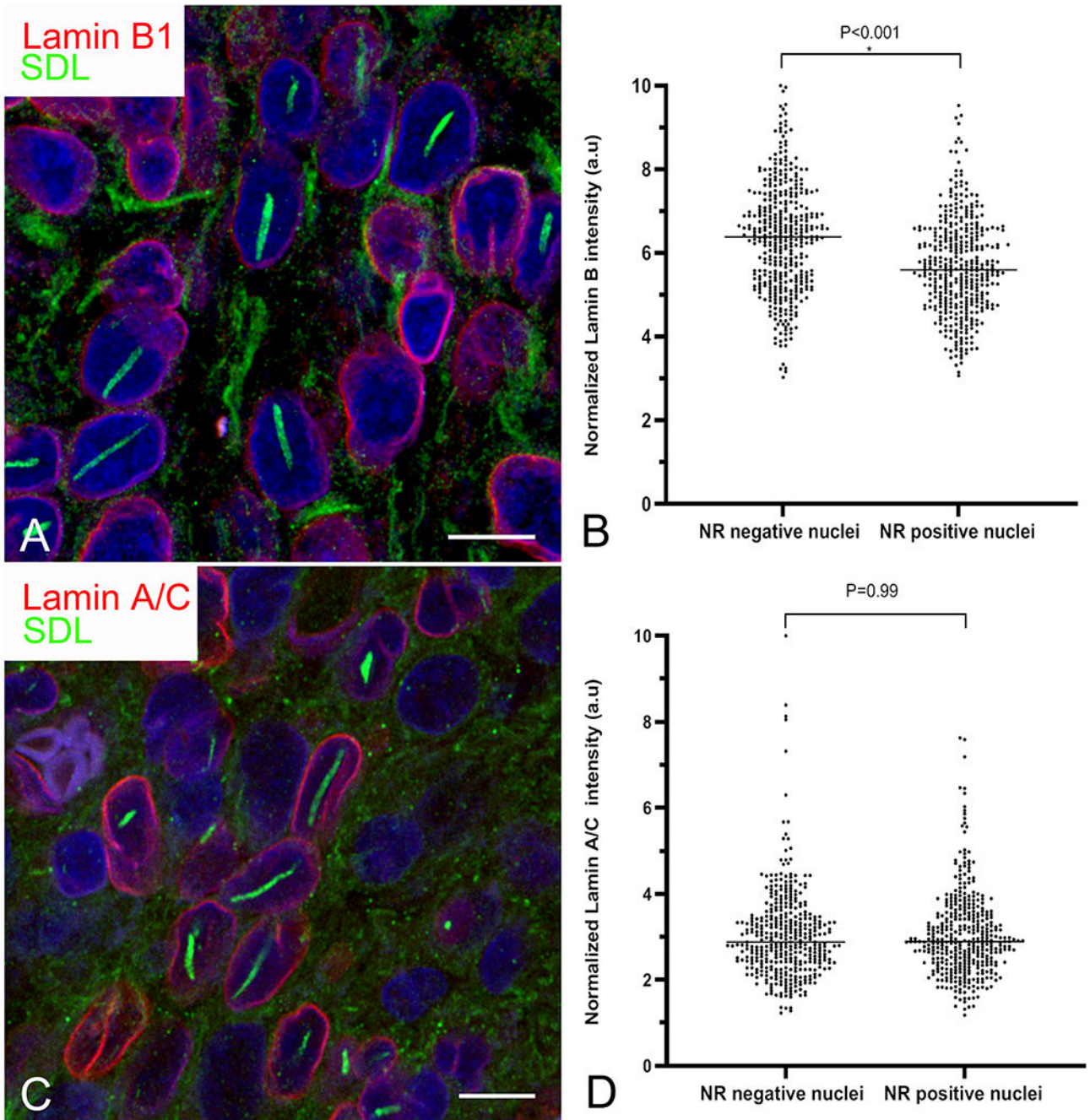


Figure 5:

Rods are associated with selective depletion of lamin B1. A, C) Confocal images of an oligodendrogloma showing visibly reduced lamin B1 (A; red) but not lamin A/C (C; red) staining intensity in cells with rods (green). Bars=10 μ m. B, D) Grouped scatter plots of pooled data from astrocytomas and oligodendroglomas showing significantly reduced staining intensity for lamin B1 (B) but not lamin A/C in cells with nuclear rods (NR).

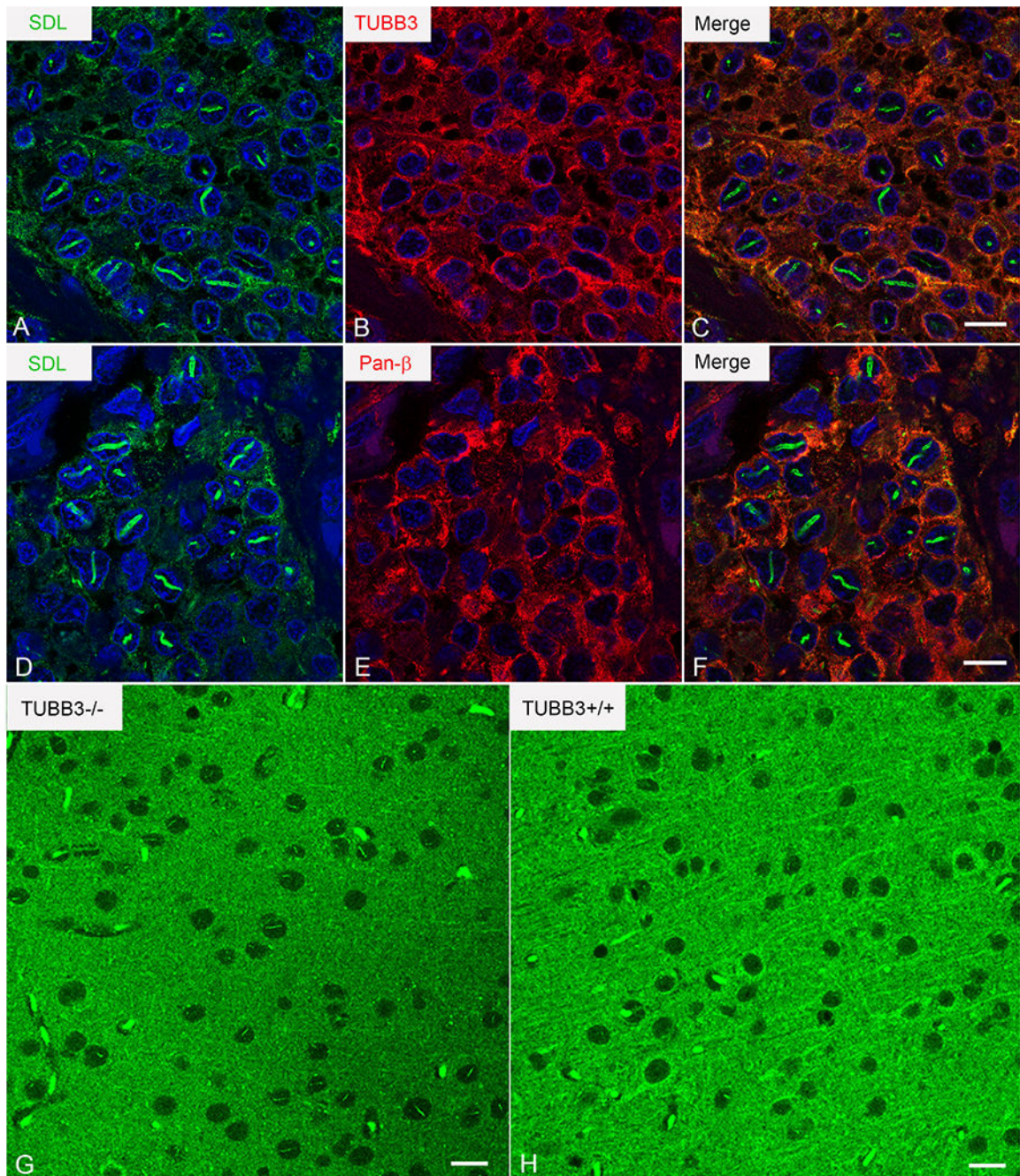


Figure 6:

Rod antigenicity: SDL does not recognize TUBB3 in rods A-F) SDL-immunoreactive rods (A, D; green) show no staining for TUBB3 using an anti-TUBB3 polyclonal antibody (B; red) or pan- β -tubulin using a rabbit monoclonal antibody (E, red). Merged images in C and F. G, H) SDL stains rods in *Tubb3*-null mice. Confocal images of the mesial frontal cortex of *Tubb3*^{-/-} (G) and *Tubb3*^{+/+} (H) mice immunostained using SDL.3D10. Bars=10 μ m in C and F and 15 μ m in G and H.

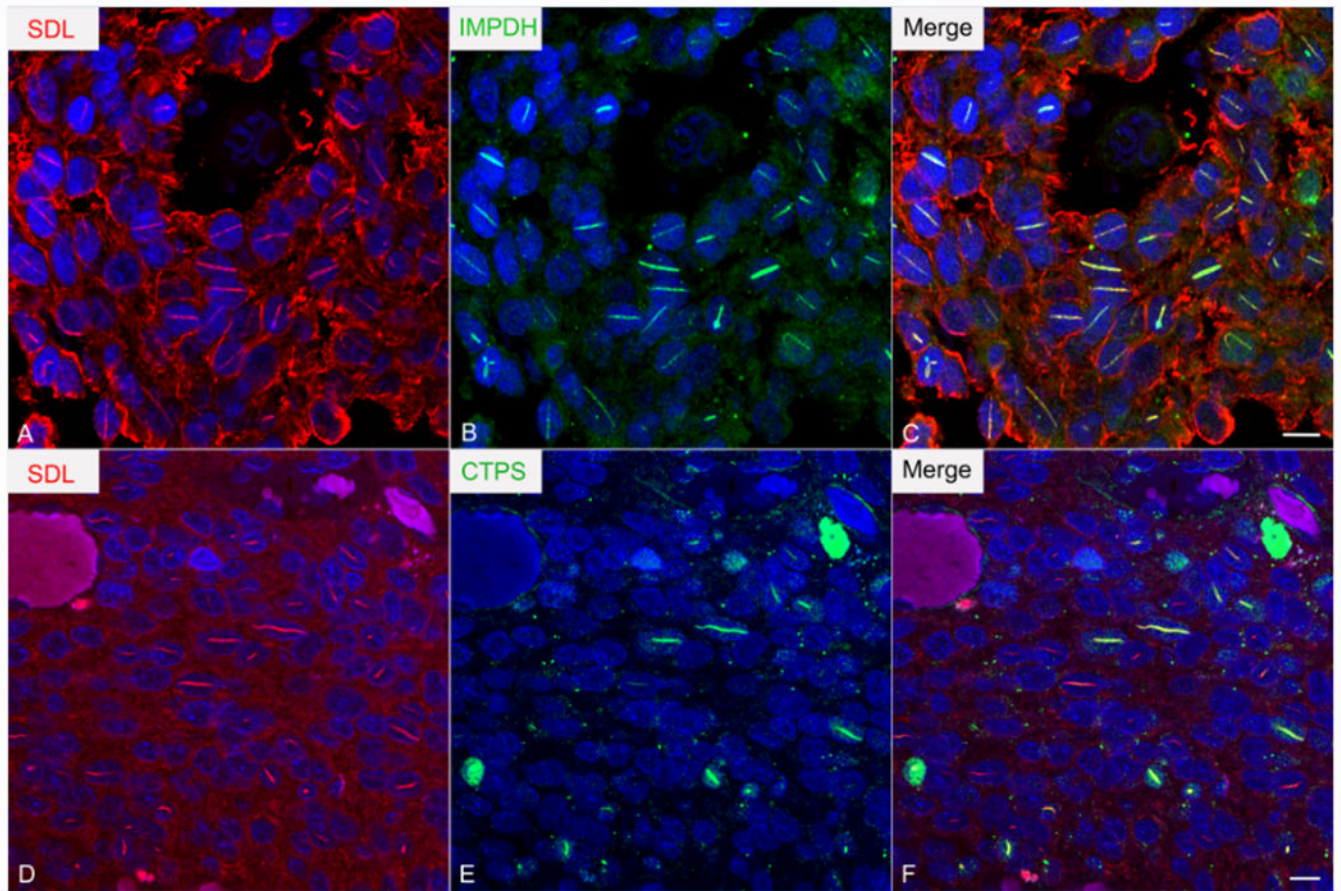


Figure 7: Rods are immunoreactive for IMPDH and CTPS. Double immunofluorescence of an oligodendrogloma showing co-localization of IMPDH (A; green) and CTPS (D; green) with SDL (B, E; red) in rods. Merged images in C and F. Bars=10 μ m.

Table 1

Primary antibodies used in the study

Antibody	Clone	Host	Dilution	Source	Product #
TUBB3	SDL.3D10	mouse monoclonal	1:100	Millipore Sigma, Burlington, MA, USA	T8660
TUBB3	TUJ1	mouse monoclonal	1:200	Biologend, San Diego, CA, USA	801213
TUBB3	TU20	mouse monoclonal	1:500	Millipore Sigma, Burlington, MA, USA	MAB1637
TUBB3	N/A	rabbit polyclonal	1:2000	Biologend, San Diego, CA, USA	802001
TUBB (pan)	EPR16774	rabbit monoclonal	1:200	Abcam, Cambridge, UK	ab179513
TUBA	EP1332Y	rabbit monoclonal	1:250	Abcam, Cambridge, UK	ab52866
IMPDH1	N/A	rabbit polyclonal	1:50	Proteintech, Rosemont, IL, USA	22092-1-AP
IMPDH1	F-6	mouse monoclonal	1:50	Santa Cruz, Dallas, TX, USA	sc-166551
IMPDH2	N/A	rabbit polyclonal	1:200	Proteintech, Rosemont, IL, USA	12948-1-AP
CTPS1	N/A	rabbit polyclonal	1:200	Abcam, Cambridge, UK	ab244492
CTPS2	EPR16735	rabbit monoclonal	1:400	Abcam, Cambridge, UK	ab196016
Ki67	SP6	rabbit monoclonal	1:100	Abcam, Cambridge, UK	ab16667
Lamin B1	N/A	rabbit polyclonal	1:200	Abcam, Cambridge, UK	ab16048
Lamin A/C	EPR4100	rabbit monoclonal	1:250	Abcam, Cambridge, UK	ab108595